

830 nm Emission in Sodium Vapor

W. T. Luh, Yan Li, and J. Huennekens

Department of Physics, Lehigh University, Bethlehem, PA 18015, USA

Received 13 March 1989/Accepted 17 April 1989

Abstract. We demonstrate that the intriguing 830 nm coherent emission, which is observed when sodium vapor is pumped with a high-power pulsed laser tuned near the $3S \rightarrow 4D$ two-photon transition, is due to an axially phase-matched six-wave mixing process. This conclusion is based upon the observation of emission near 584 nm, which is coupled to the 830 nm emission in the six-wave mixing process: $\omega_1 + \omega_2 = 2\omega_L - \omega_{4D \rightarrow 4P} - \omega_{4P \rightarrow 3D}$. In addition, we have observed coherent emission near $1.16 \mu\text{m}$, which is due to an analogous process involving cascade through the $4S$ (as opposed to the $3D$) state. We calculate the wavelengths of all photons involved in these processes using the standard formulas of parametric wave-mixing theory, and show that they can be predicted to within experimental uncertainties. Finally we report observations of significant blue shifts of the 830 nm and $1.16 \mu\text{m}$ emissions in a mixed sodium-potassium vapor. These shifts can be readily understood by considering the effect of the potassium on the frequency-dependent refractive index of the vapor. Due to these results, other recent interpretations of the 830 nm emission as stimulated excimer emission on the Na_2 $1^3\Sigma_g^+ \rightarrow 1^3\Sigma_u^+$ band must now be rejected.

PACS: 42.65.Ky

When alkali vapors are pumped by high-power lasers tuned near two-photon allowed atomic transitions, a number of coherent and stimulated emissions can be observed. These include optically pumped stimulated emission (OPSE), stimulated hyper-Raman scattering (SHR), amplified spontaneous emission (ASE) and angle phase-matched four- and six-wave mixing (see [1–7] and references therein for an introduction to the growing literature in this field). Recently, axially phase-matched four- and six-wave mixing in sodium vapor excited near the $3S \rightarrow 3D$, $4D$ two-photon transitions has been identified experimentally and explained theoretically [8,9]. In addition to these atomic processes, the laser frequency may overlap one or more ro-vibrational transitions of the alkali molecules that are also present in the vapor. This can result in dimer lasing (or more correctly ASE in the absence of an optical cavity) on the bound-bound electronic transitions [10–12].

The present study concerns the strong coherent emission at 830 nm which is observed when sodium vapor is pumped near the $3S \rightarrow 4D$ two-photon transition. This emission has been the subject of several

studies over the last several years, the first of which (to the best of our knowledge) being that of Dinev et al. [13]. These authors identified the 830 nm emission as excimer lasing on the Na_2 $1^3\Sigma_g^+ \rightarrow 1^3\Sigma_u^+$ bound-free transition since the emission spectrum appears broad and band-like and since this particular triplet band is the only known atomic or molecular emission which occurs in sodium vapor in this wavelength region [14,15]. In addition, they identified a sharp feature near 840 nm, which occurs under the same experimental conditions, as a bound-bound cascade transition involving higher molecular states. The proposed mechanism involves collisional excitation transfer from the $4D$ excited state to a highly-excited bound triplet state of Na_2 . The molecule then cascades in bound-bound stimulated transitions (one of them producing the 840 nm emission) down to the lowest vibrational level of the $1^3\Sigma_g^+$ state. The 830 nm emission results from the bound-free $1^3\Sigma_g^+ \rightarrow 1^3\Sigma_u^+$ transition, which is the final step of the cascade.

A later study by Wang et al. [6] showed that the 840 nm emission was actually an angle phase-matched six-wave mixing process satisfying the energy conser-

vation equation

$$\omega_{840} = 2\omega_L - (\omega_{4D \rightarrow 4P} + \omega_{4P \rightarrow 3D} + \omega_L) \quad (1)$$

and the momentum conservation equation

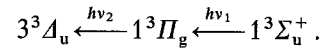
$$\mathbf{k}_{840} = 2\mathbf{k}_L - (\mathbf{k}_{4D \rightarrow 4P} + \mathbf{k}_{4P \rightarrow 3D} + \mathbf{k}_L), \quad (2)$$

where ω_L and \mathbf{k}_L are the laser frequency and wave vector. Since in general $\mathbf{k} = (n\omega/c)\hat{k}$ where n is the (frequency dependent) index of refraction, (1) and (2) can only both be satisfied if the 840 nm emission propagates in a cone centered on the pump laser axis (Fig. 1a). Under the same experimental conditions that produced the 830 and 840 nm emissions, Wang et al. also observed Na_2 $1(A)^1\Sigma_u^+ \rightarrow 1(X)^1\Sigma_g^+$ stimulated emission in the region between 784 and 800 nm [Ref. 6, Fig. 4]. This is due to the fact that the laser, which is tuned near the $3S \rightarrow 4D$ two-photon atomic transition, coincidentally also pumps various $1^1\Sigma_u^+ \leftarrow 1^1\Sigma_g^+$ rovibrational transitions. In an interesting experiment, Wang et al. were able to completely suppress the dimer emissions by superheating the vapor using a hot wire passing down the axis of their heat-pipe oven parallel to the pump beam axis. This superheating, which decreased the number of bound dimers thereby dropping the $1^1\Sigma_u^+ \rightarrow 1^1\Sigma_g^+$ stimulated emission below threshold, did not affect either the 830 or the 840 nm emission intensity. This led to the conclusion that the 830 nm emission was probably not due to any process which involved the bound, ground state molecules. In addition, they showed that placing the oven inside an optical cavity enhanced the dimer emission near 790 nm but not the emissions at 830 and 840 nm. Although it was not possible to rule out the excimer explanation of the 830 nm emission as a result of these experiments (since bound $1^3\Sigma_u^+$ molecules and colliding atom pairs interacting along the $1^3\Sigma_u^+$ potential curve would not be depleted by the superheating), Wang et al. concluded from the strong similarities to the 840 nm signals and other evidence, such as the strong forward to backward emission asymmetry, that the 830 nm emission was probably also an atomic parametric process.

Very recently, Bajic et al. [16] reported new experimental data on the 830 nm emission, and concluded that it was indeed stimulated excimer emission on the $1^3\Sigma_g^+ \rightarrow 1^3\Sigma_u^+$ band of Na_2 . This conclusion was based on the broad excitation spectrum (see [Ref. 16, Fig. 5] or Fig. 5 of the present work) which shows a pronounced dip at the two-photon atomic frequency (thus suggesting that the excitation is of a molecular or quasi-molecular nature). Bajic et al. proposed that the excitation occurred through the two-photon process $3^3A_u \xleftarrow{2h\nu} 1^3\Sigma_u^+$. In addition, for some experimental conditions, the spectrum of the 830 nm emission is

much broader than is typical for other atomic parametric processes such as the 840 nm peak. Finally, Bajic et al. argue that they have observed an analogous emission peak in potassium vapor, which they attribute to the $1^3\Sigma_g^+ \rightarrow 1^3\Sigma_u^+$ excimer band of the K_2 molecule.

We became interested in the 830 nm emission due to our long term interest in the alkali excimer bands, and in possibilities for producing tunable, near-infrared lasers based upon them. The evidence regarding an excimer as opposed to an atomic parametric explanation for the 830 nm emission seemed inconclusive to us, so we decided to carry out a two-color excitation experiment (suggested by Wang et al. in their paper) to test this hypothesis. If the excimer explanation was correct, we believed the 830 nm emission could be resonantly enhanced through the pumping scheme



Here laser 1 would be tuned near 551.5 nm, which is the wavelength of the well localized $1^3\Pi_g \leftarrow 1^3\Sigma_u^+$ satellite [17], while laser 2 would be tuned near 609.1 nm, which is the wavelength needed to bring the two-photon sum close to the $3S-4D$ energy separation.

However, before we got to the two-color experiment, we obtained new data from a one-laser experiment which we believe unambiguously identifies the 830 nm emission as resulting from an axially phase-matched six-wave mixing process. Processes of this type have been described in detail by Moore et al. in an interesting paper which appeared recently [8]. In axially phase-matched wave-mixing, the photons all propagate collinearly with the pump beam (Fig. 1b). In this case, and for the particular six-wave process which is of interest here (Fig. 2), the energy and momentum conservation equations become:

$$\omega_1 + \omega_2 = 2\omega_L - (\omega_{4D \rightarrow 4P} + \omega_{4P \rightarrow 3D}) \quad (3)$$

and

$$|\mathbf{k}_1| + |\mathbf{k}_2| = 2|\mathbf{k}_L| - (|\mathbf{k}_{4D \rightarrow 4P}| + |\mathbf{k}_{4P \rightarrow 3D}|). \quad (4)$$

Here ω_1 and ω_2 (and the corresponding wave vectors) refer to the two axially phase-matched waves produced in the vapor which satisfy (3) and (4). In the following sections of this article, we present our data on the 830 nm, and other related coherent emissions. In particular, we have observed both ω_1 and ω_2 for the process described by (3) and (4), as well as for an analogous process involving the $\text{Na } 4S$ (as opposed to the $3D$) state (Fig. 2). Section 1 of this paper describes our experimental set-up. Section 2 presents our experimental results which include emission and excitation

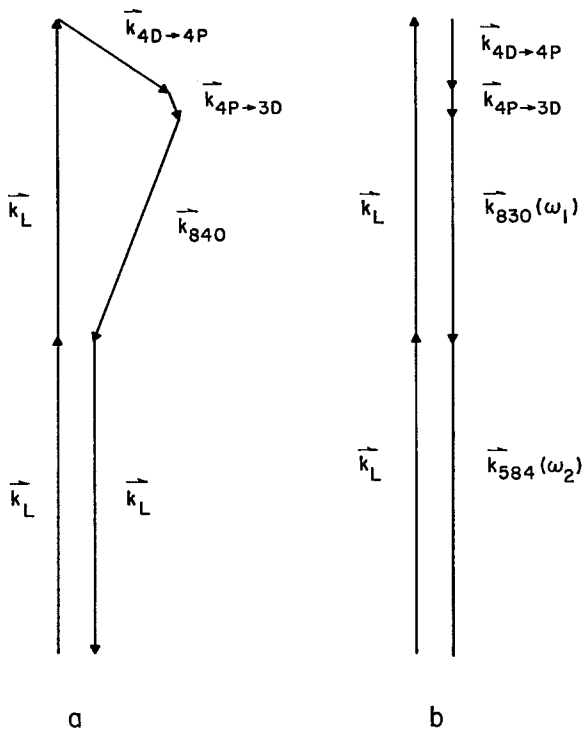


Fig. 1a, b. Phase matching diagrams for six-wave mixing processes occurring in sodium vapor pumped at the $3S \rightarrow 4D$ two-photon transition wavelength. **a** Angle phase-matched process described by (1) and (2). The angles have been greatly exaggerated for clarity. **b** Axially phase-matched process described by (3) and (4)

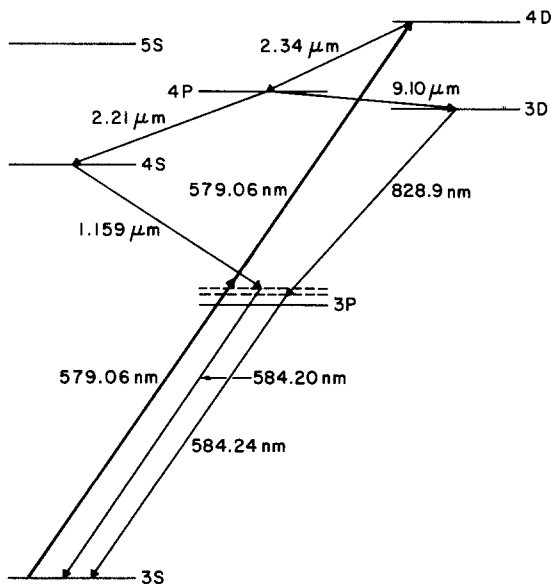


Fig. 2. Partial energy level diagram of sodium showing the two axially phase-matched six-wave mixing processes studied in the present work. In this example, the pump laser (which is indicated by the heavy lines) is tuned to 579.06 nm (with respect to air), which is near to the $3S \rightarrow 4D$ two-photon transition. The other wavelengths given in the figure correspond to this pump wavelength. The separation of the two virtual levels above the $3P$ state is greatly exaggerated. Energies are taken from [18]

scans, laser power dependences, angle dependences of the emission, etc. Section 3 contains theoretical calculations of the wavelengths of the observed axially phase-matched six-wave mixing processes in both pure sodium and in mixed sodium-potassium vapor. Finally, Sect. 4 presents our conclusions and a summary.

1. The Experiment

Figure 3 shows a diagram of the experimental set-up. A frequency-doubled Nd:YAG laser (Quanta Ray DCR 11) with an output power of ~ 100 mJ was used to pump a commercial Littman-type dye laser (Lumonics HyperDye 300). The dye laser was operated with Rhodamine 6G dye and produced output powers of ~ 6 mJ in a pulse of ~ 6 ns duration. The linewidth was ~ 0.1 cm^{-1} .

The dye laser was tuned near 579 nm (i.e. close to the sodium $3S \rightarrow 4D$ two-photon transition wavelength), and was used to excite sodium vapor contained in a heat-pipe oven. Two ovens were used for the present experiment. The first is a linear heat-pipe containing pure sodium metal, while the second is a four-armed cross containing sodium-potassium mixtures. Both ovens were typically operated at ~ 770 K, which corresponds to a sodium vapor pressure of ~ 5.5 mbar. In the pure sodium pipe, the argon buffer gas pressure was ~ 16 mbar, but was raised to 33–47 mbar in the Na–K mixture.

The laser beam was directed through the heat-pipe oven and onto the entrance slits of a 0.75 m monochromator (Spex model 1702). Coherent and stimulated emissions emerging from the alkali vapor along the pump laser axis were then also aligned to the monochromator slits. Color glass and interference filters were used in front of the monochromator to eliminate second and higher order grating effects, and

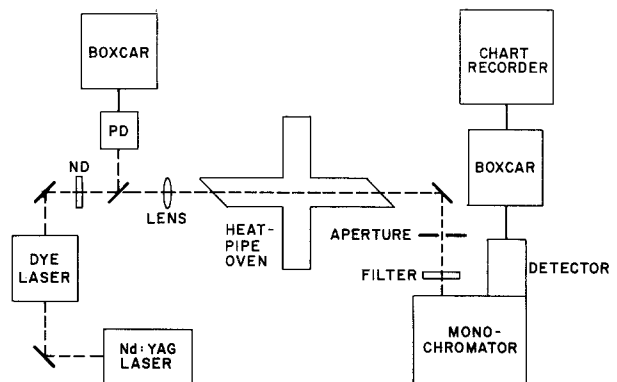


Fig. 3. Experimental set-up. ND and PD represent neutral density filter and photodiode, respectively

to filter out the strong pump laser light before it reached the detector. An aperture was placed along the beam path approximately 0.7 m from the exit window. This was used to study the angular divergences of the various emissions of interest. Neutral density filters were used before the heat-pipe to control the pump laser intensity which was monitored continuously with a photodiode. A lens was used to focus the laser to a diameter of $\sim 0.5\text{--}1.0$ mm in the center of the oven.

The dispersed emission spectra exiting the monochromator were detected by either an S-1 or S-20 photomultiplier (Hamamatsu R1767 or R1387, respectively), whose output was sent to a gated boxcar-averager (Stanford Research SR250). The boxcar signals were recorded on a strip-chart recorder or laboratory computer.

Typically, data were taken in two modes. For emission spectra, we set the laser to a particular frequency and scanned the monochromator. Excitation spectra were obtained by setting the monochromator transmission wavelength and scanning the laser wavelength. Depending on the detection efficiency for the wavelength of interest and the proximity of that wavelength to the pump laser line, monochromator slits were adjusted to give a resolution between 0.2 and 0.8 nm.

2. Experimental Results

In Fig. 4 we show forward emission spectra for the various wavelength ranges of interest. Details of the emission spectra depend on the exact laser wavelength, although the main features are the same for all excitation wavelengths near the $3S \rightarrow 4D$ two-photon transition. Here, the pump laser wavelength was set to 578.76 nm. Part b) of the figure shows the 830 nm emission along with the unresolved $3D \rightarrow 3P$ atomic ASE and other processes near 820 nm, and the angle phase-matched wave-mixing signal at 840 nm. Part c) shows the analogous region near the $4S \rightarrow 3P$ transition wavelength. The peaks near 1.14 μm correspond to the $4S \rightarrow 3P$ fine-structure doublet, while that at 1.18 μm is the analog of the 840 nm emission which has previously been reported by Hartig [2]. Clearly, the 1.16 μm peak appears to be the analog of the 830 nm axially phase-matched emission. This conclusion will be justified in the next section where we will calculate the expected positions of the various emission lines which result from the axially phase-matched six-wave processes. The observed positions of the 830 nm and 1.16 μm peaks are compared in Table 1 with values calculated as described in the next section. According to theory, the 1.16 μm and 830 nm emission should be

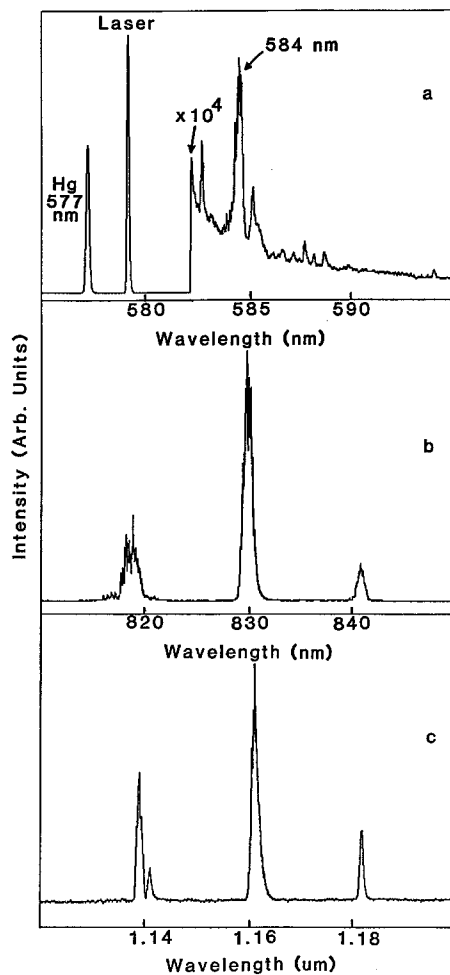


Fig. 4a-c. Forward emissions scans obtained in pure sodium vapor with the laser tuned to 578.76 nm, which is near the sodium $3S \rightarrow 4D$ two-photon transition. Part a shows the region between 575 and 595 nm, which includes a mercury calibration line, the laser line, and the axial emission at 584 nm. The laser line was attenuated by $\sim 10^4$. Monochromator slits were adjusted to 30 μm (yielding a resolution of ~ 0.2 nm) in order to distinguish the 584 nm emission from leakage through the monochromator of the very strong laser line (which is responsible for the background near 584 nm). We demonstrated that the other small peaks near the 584 nm line are grating ghosts, but that the 584 nm peak itself is not. Part b shows the region from 810–850 nm which includes the $3D \rightarrow 3P$ ASE and wave-mixing signals near 819 nm, the axially phase-matched emission near 830 nm, and the angle phase-matched emission near 840 nm. Part c contains the region between 1.12 and 1.20 μm , which shows the analogous $4S$ state channel. The monochromator slits were 300 μm in parts b and c. In all parts, the heat pipe oven temperature and buffer gas pressure were $\sim 510^\circ\text{C}$ and ~ 16 mbar, respectively. The laser energy was ~ 1 mJ in a 6 ns pulse.

coupled to emission at a wavelength which is roughly halfway between the wavelengths of the laser and the $3P \rightarrow 3S$ atomic line (Fig. 2). Figure 4a shows an emission scan taken in the region around 584 nm. A clear peak is observed close to the predicted position (see

Table 1. Observed and calculated wavelengths for axially phase-matched six-wave mixing processes occurring in pure sodium vapor excited at the $3S \rightarrow 4D$ two-photon transition. All wavelengths are taken in air, and are expressed in nm. Experimental uncertainties are given in parentheses

	λ_{pump}	3D channel		4S channel	
		$\lambda(\omega_1)$	$\lambda(\omega_2)$	$\lambda(\omega_1)$	$\lambda(\omega_2)$
Exp.	578.66 (± 0.05)	—	829.66 (± 0.3)	—	1160.55 (± 0.5)
Calc.		584.05	829.24	584.00	1159.69
Exp.	578.76	584.00	829.16	584.00	1160.34
Calc.		584.10	829.15	584.05	1159.48
Exp.	578.86	583.90	829.04	583.90	1160.31
Calc.		584.15	829.05	584.10	1159.30
Exp.	579.06	584.26	828.96	584.26	1159.09
Calc.		584.24	828.86	584.20	1158.92

also Table 1). Although this peak is difficult to isolate due to its proximity to the laser line, we were able to demonstrate that the observed peak is not a grating ghost or other artifact. The excitation spectra and power dependences, which will be presented next, support our identification of this 584 nm emission as the final photon in the axially phase-matched six-wave mixing process.

Figure 5 shows the excitation spectra for the 584 nm, 830 nm, and 1.16 μm axially phase-matched six-wave mixing signals. It is important to note that the detailed shapes of the excitation spectra depend critically on the wavelength setting of the monochromator, and on the monochromator slit widths. [Ref. 16, Fig. 5] presents excitation spectra for several different monochromator wavelength settings near 830 nm, which are consistent with our observations. Nevertheless, the strong similarity of the 584 nm, 830 nm, and 1.16 μm excitation spectra is strong evidence that these emissions are closely related. In particular, all show a pronounced dip exactly at the $3S \rightarrow 4D$ two-photon transition wavelength, regardless of the monochromator setting. Figure 6 shows for comparison the excitation spectra of the 820 nm, 830 nm (axially phase-matched six-wave mixing), and 840 nm (angle phase-matched six-wave mixing) signals, as well as those of the analogous lines from the 4S state channel. The 820 nm and 1.14 μm signals consist of both ASE and parametric wave-mixing emissions resulting in

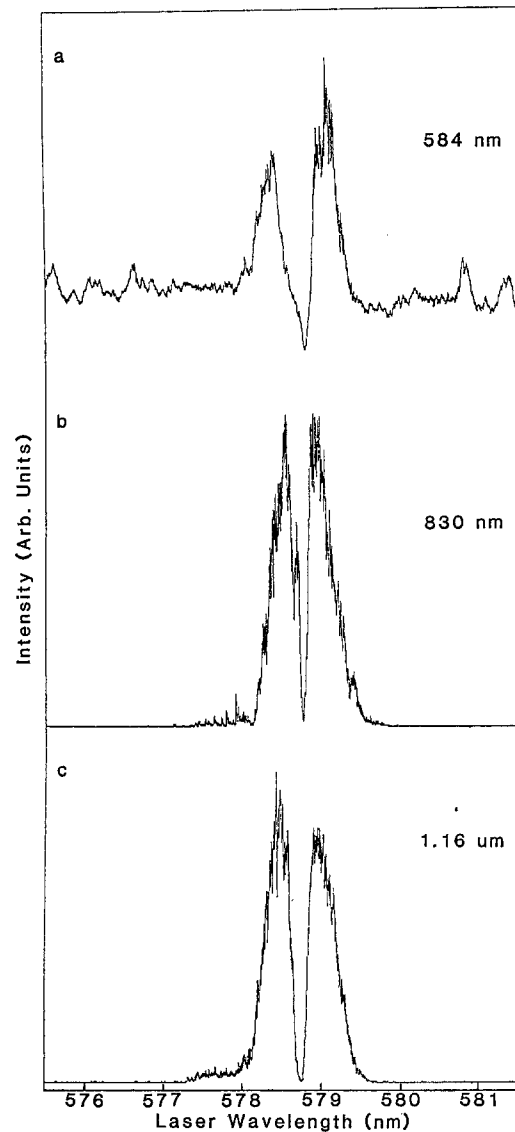


Fig. 5a–c. Laser excitation spectra for axial emission at **a** 584 nm **b** 830 nm and **c** 1.16 μm . Monochromator slits were set to 30 μm for part **a**, and 300 μm for parts **b** and **c**. The oven was operated with pure sodium, and the temperature and pressure were $\sim 550^\circ\text{C}$ and ~ 16 mbar, respectively. Laser power was ~ 2 mJ

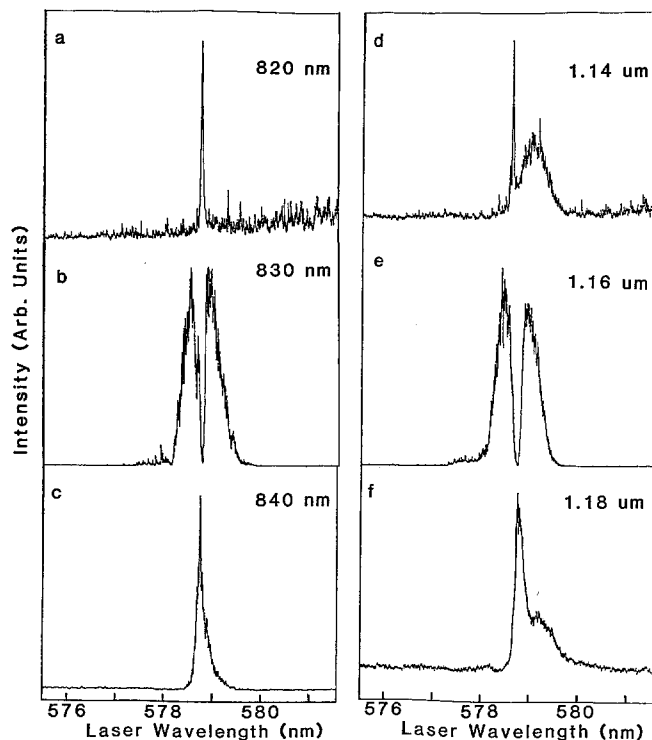


Fig. 6a-f. Laser excitation spectra in pure sodium vapor for processes coupled to the 3D states: **a** ASE and wave-mixing at 819 nm, **b** axially phase-matched emission at 830 nm, and **c** angle phase-matched emission at 840 nm. **d, e, and f** Excitation spectra for analogous processes coupled to the 4S state, at 1.14, 1.16, and 1.18 μm , respectively. The oven temperature and buffer gas pressure were $\sim 550^\circ\text{C}$ and ~ 16 mbar, respectively. Monochromator slits were 30 μm for part **a**, and 300 μm for parts **b** through **f**. The laser power was ~ 2 mJ

complicated excitation spectra which depend strongly on the monochromator wavelength and slitwidth. In particular, the 820 nm signal shows only a sharp spike on resonance because of the narrow slits used in part **a**) of Fig. 6 (which were needed to discriminate against unwanted molecular emissions). With wider slits at lower pressures, the 820 nm excitation spectrum shows a broad hump to the red of the narrow spike, and is thus quite similar to the 1.14 μm excitation spectrum presented in Fig. 6d. We did not investigate these features any further in the present work, since these emissions have been well studied previously [8]. All of the spectra shown in Fig. 6 change in detail as the monochromator wavelength is varied. However, the purpose of Figs. 5 and 6 is to demonstrate the qualitative similarity of the 584 nm, 830 nm, and 1.16 μm excitation spectra, and to point out their marked differences from those of the ASE and angle phase-matched processes.

Figure 7 presents the dependences of the various observed signals on pump laser power. Again, the similarity of the 584 nm, 830 nm, and 1.16 μm emis-

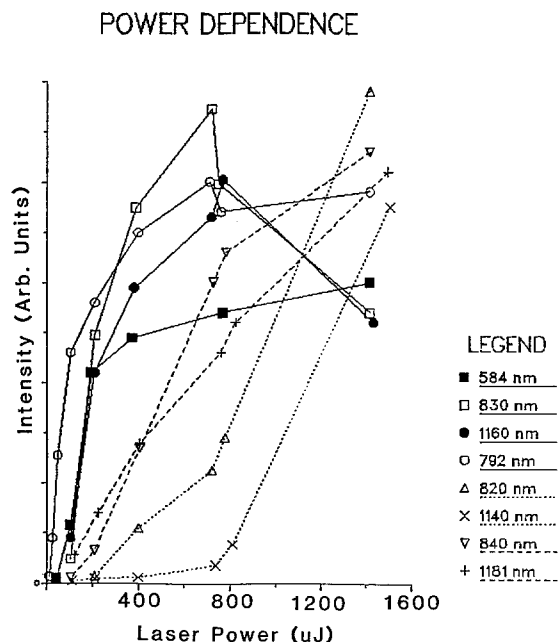


Fig. 7. Dependence of the forward emission intensities on pump laser power for the various processes studied in this work. Dotted curves represent the ASE and wave-mixing signals at 820 nm and 1.14 μm . Dashed curves correspond to angle phase-matched processes at 840 nm and 1.18 μm . Solid lines correspond to the axially phase-matched emissions at 584 nm, 830 nm, and 1.16 μm . The power dependence of stimulated emission on one Na_2 dimer line at 792 nm is also shown as a solid line for comparison. The oven contained pure sodium vapor and was operated at a temperature and buffer gas pressure of $\sim 500^\circ\text{C}$ and ~ 17 mbar, respectively. The laser wavelength was 578.70 nm

sions (shown as solid lines in the figure) can be seen. The angle phase-matched signals at 840 nm and 1.18 μm (dashed lines) also behave similarly to each other, as do the signals at 820 nm and 1.14 μm (dotted curves). This figure also includes the power dependence of one Na_2 $1^1\Sigma_u^+ \rightarrow 1^1\Sigma_g^+$ band OPL line at 792 nm (also shown as a solid line) for comparison [6, 11].

While Fig. 7 presents the dependences of the various emission peaks on pump laser intensity, Fig. 8 shows the variation of the full 830 nm excitation spectrum with laser intensity. Note that the resonance dip becomes narrower and the overall width of the excitation peak decreases as the laser intensity is reduced. These dependences are not yet well understood, but we will discuss some possible explanations in the next section.

Additional information can be obtained from angle dependent studies similar to those carried out by Moore et al. [8, 9]. Figure 9 shows the emission in the 810–850 nm region with the aperture in Fig. 3 fully opened (Fig. 9a) and partially closed (Fig. 9b). It can be seen that the 830 nm emission is concentrated more

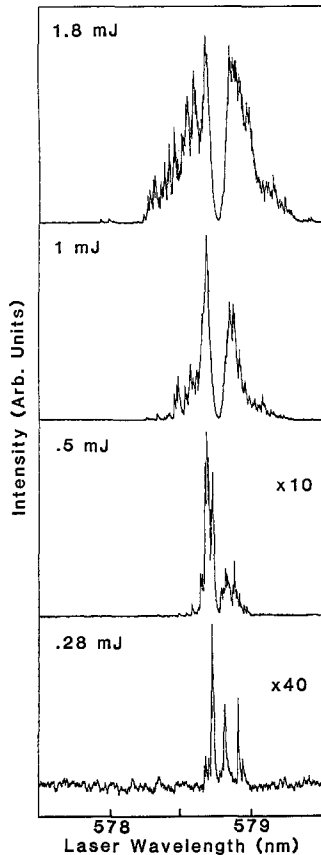


Fig. 8. Laser power dependence of the 830 nm excitation spectrum in pure sodium vapor. Oven temperature and pressure were $\sim 550^\circ\text{C}$ and ~ 16 mbar, respectively. For these scans, the monochromator wavelength was set to 829.9 nm, and the slits to 100 μm

closely along the pump laser axis than the angle phase-matched emission at 840 nm, or the combination of processes which contribute to the peak at 820 nm.

Finally, we present in Fig. 10 emission spectra taken in mixed sodium-potassium vapor. Note that the 830 nm emission has shifted to ~ 825 nm in the mixture. The frequency of the 1.16 μm peak (not shown in the figure) also shifts, but by a lesser amount. These observed shifts were the most important clue in leading us toward an axial phase-matched wave-mixing explanation for these processes. The shifts can be predicted from the simple model presented in the next section.

3. Theoretical Treatment

Figure 2 presents an energy level diagram for sodium. In the figure, we show two paths which can be described as axially phase-matched six-wave mixing. In the following, we will show that the channel involving the 3D state is responsible for the sodium 830 nm emission.

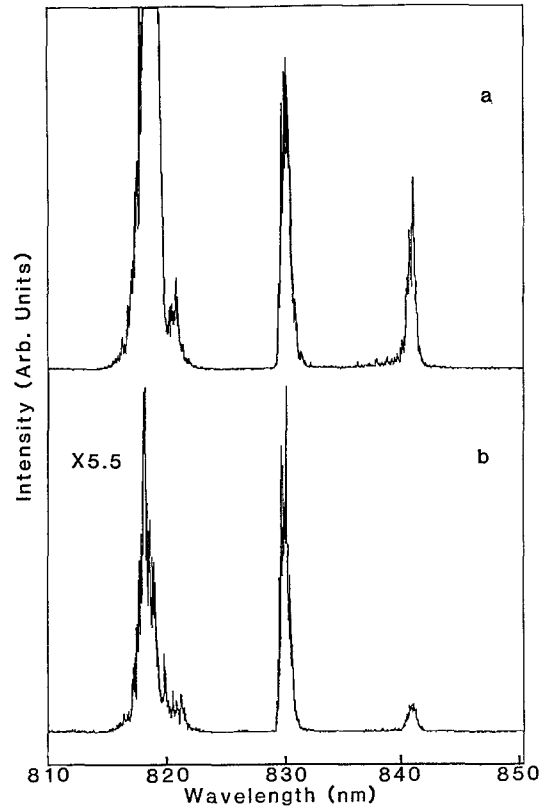


Fig. 9. **a** Forward emission scan in the 810–850 nm region obtained with the aperture in Fig. 2 fully opened. **b** Same spectrum but with the aperture partially closed. In part **b**, the sensitivity is 5.5 times greater. It can be seen that the intensities of the 820 and 840 nm emissions are reduced much more by the aperture than is the 830 nm emission. Thus these spectra demonstrate that the 830 nm emission is concentrated more closely to the laser axis than are the other two emissions. For these scans, the pure sodium oven temperature and buffer gas pressure were $\sim 510^\circ\text{C}$ and ~ 16 mbar, respectively. The laser power was ~ 1.2 mJ. The laser wavelength was 578.66 nm

The theory of axially propagating parametric wave-mixing has been discussed in some detail by Moore et al. [8]. In the case of alkali vapors, it is straight-forward to calculate the wavelengths of the two parametric waves produced in axial four- or six-wave mixing processes. For the particular case of axially phase-matched six-wave mixing produced by two-photon pumping of the sodium $3S \rightarrow 4D$ transition, we can calculate these wavelengths as follows. Using the relation $|\mathbf{k}| = \omega n/c$, where n is the refractive index at the relevant frequency, we can combine (3) and (4) to yield:

$$\begin{aligned} & \omega_1[n(\omega_1) - 1] + \omega_2[n(\omega_2) - 1] \\ & = 2\omega_L[n(\omega_L) - 1] - \omega_{4D \rightarrow 4P}[n(\omega_{4D \rightarrow 4P}) - 1] \\ & \quad - \omega_{4P \rightarrow 3D}[n(\omega_{4P \rightarrow 3D}) - 1]. \end{aligned} \quad (5)$$

The frequency dependent index of refraction is in general given by $n = \text{Re}\{\epsilon^{1/2}\}$ with ϵ the dielectric constant obtained from the expression: [19]

$$\frac{\epsilon - 1}{\epsilon + 2} = \frac{4\pi e^2}{3m} \sum_{i,k} N_i \frac{f_{ik}}{\omega_{ik}^2 - \omega^2 - i\gamma_{ik}\omega}. \quad (6)$$

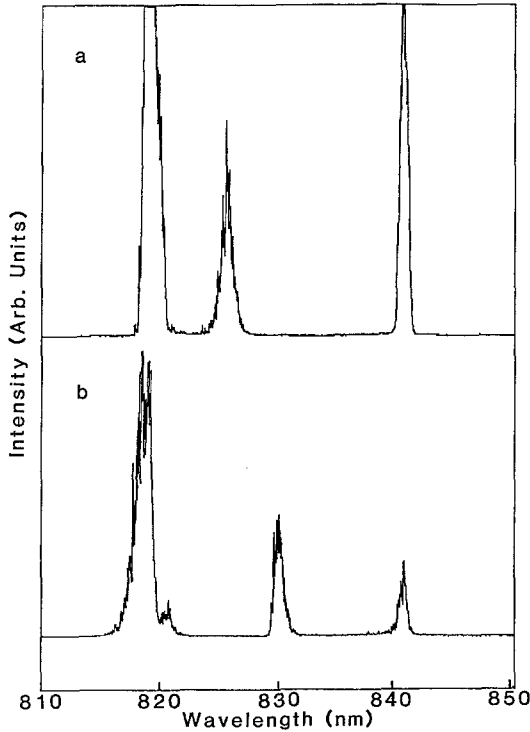


Fig. 10a, b. Emission scans of the 810–850 nm region obtained in **a** a mixed sodium-potassium vapor and **b** in pure sodium, with the laser tuned to 578.66 nm. The oven temperature was $\sim 510^\circ\text{C}$ for the pure vapor, and varied with position over the range $370\text{--}500^\circ\text{C}$ in the mixed vapor. The buffer gas pressure was ~ 36 and 16 mbar in parts **a** and **b**, respectively. The laser power was ~ 1.2 mJ

Here e and m are the charge and mass of the electron, ω_{ik} , f_{ik} , and γ_{ik} are the frequency, oscillator strength, and half-width (FWHM) of the transition from state i to state k , and we are considering the case of pure sodium vapor. For $n \sim 1$ in a dilute gas, and outside of the resonance linewidths ($|\omega - \omega_{ik}| \gg \gamma_{ik}$), this expression reduces to: [3, 19]

$$n - 1 \approx 2\pi \frac{e^2}{m} \sum_{i,k} N_i \frac{f_{ik}}{\omega_{ik}^2 - \omega^2}. \quad (7)$$

If we now make the assumption that the populations in the excited states are small, we need only consider transitions from the ground state. Thus we can eliminate the sum over i in (7), and replace N_i by the total atom density N . In the case of sodium, the sum over k is just the resonance series of $S \rightarrow P$ transitions. For our situation of six-wave mixing, all photon wavelengths of interest are greater than 578 nm, so the $3S \rightarrow 3P$ transitions at 589.0 and 589.6 nm (which contain over 98% of the total oscillator strength) will dominate the sum. The next largest contribution comes from the $3S \rightarrow 4P$ transitions whose oscillator strengths are a factor of 70 smaller than those of the $3S \rightarrow 3P$ transitions. In addition, the $3S \rightarrow 4P$ transitions lie at higher frequencies ($\lambda \sim 330$ nm), so that their contributions to the right-hand side of (7) are much less than 1%.

Figure 11 shows a qualitative sketch of the function $n - 1$ in the range of interest. Since the two photons near the $4D \rightarrow 4P$ and $4P \rightarrow 3D$ transition wavelengths occur near 2.3 and 9.1 μm , respectively, the last two terms on the right-hand side of (5) will not contribute significantly. In addition, the contribution from the term on the left-hand side involving ω_2 (which will turn out to be in the vicinity of the $3D \rightarrow 3P$ transition at 820 nm), is also very small. Thus, we are left with the simple equation:

$$\omega_1 [n(\omega_1) - 1] = 2\omega_L [n(\omega_L) - 1]. \quad (8)$$

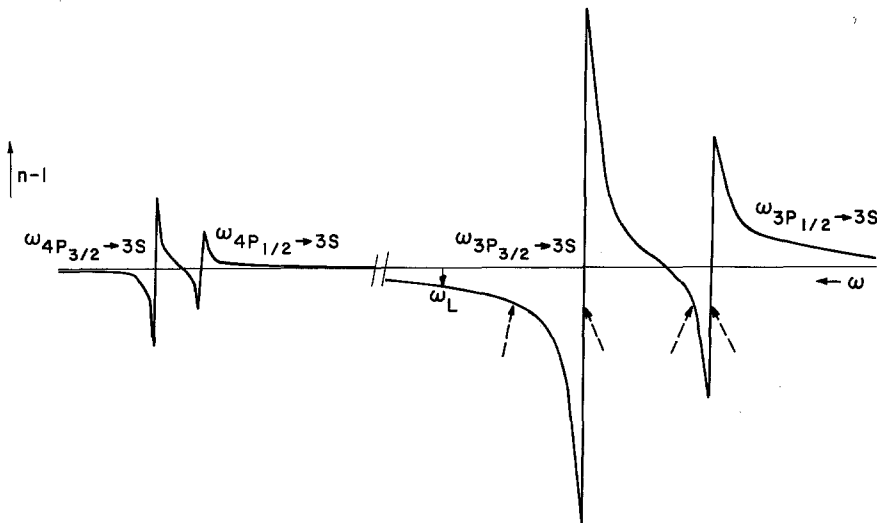


Fig. 11. Qualitative sketch of the function $n - 1$ in the regions around the sodium $3S \rightarrow 3P$ and $3S \rightarrow 4P$ transitions. The laser frequency ω_L is marked by a solid vertical arrow in the figure. The four dashed arrows represent the four points which satisfy (8) for axial phase-matching. The leftmost of the four dashed arrows is the phase-matching point at 584 nm which is also responsible for the 830 nm and 1.16 μm emissions. The figure is not drawn to scale

ω_L is marked in Fig. 11 by the solid arrow. The dashed arrows mark the four points which satisfy (8) for axial phase-matching (see also [9]). Note that two of these points occur very close to the line-centers of the $3P \rightarrow 3S$ fine-structure components. As explained in [8], these are regions of strong absorption, which tends to reduce axial wave-mixing at these frequencies. The third point, between the two $3P \rightarrow 3S$ fine-structure transition frequencies, is responsible for the axially phase-matched six-wave mixing reported in [8]. Since ω_2 is given fairly closely by:

$$\omega_2 = \omega_{3D \rightarrow 3S} - \omega_1, \quad (9)$$

this process also produces a signal at a frequency between the $3D \rightarrow 3P$ fine-structure components, which can be seen in [Ref. 8, Fig. 5].

It is the final point satisfying (8), marked by the left-most dashed arrow in Fig. 11, that is responsible for the sodium 830 nm emission. Although direct computation from (5) and (7) allows an accurate prediction of the frequencies ω_1 and ω_2 associated with this point, these frequencies can be calculated approximately from the following simple argument. Since the frequency range in the region of interest is not large, the points satisfying (8) correspond very nearly to the points where $n-1$ is simply twice $n(\omega_L)-1$. In addition, for frequency detunings that are large compared to the fine structure splitting, but not so large that $\omega \approx \omega_{3P \rightarrow 3S}$ is not a reasonable approximation, the dispersion is roughly a linear function of frequency [i.e. the frequency denominator of (7) can be approximated as

$$\omega_{3P \rightarrow 3S}^2 - \omega^2 \approx 2\omega_{3P \rightarrow 3S}(\omega_{3P \rightarrow 3S} - \omega)].$$

Therefore, it can be seen that (8) will be satisfied by one point that is close to midway between the laser and the atomic line frequencies. Since the $3D \rightarrow 3P$ atomic lines at 819 nm are the complement of the $3P \rightarrow 3S$ atomic lines, and the 840 nm emission is the complement of the laser wavelength (i.e. $\omega_{3D \rightarrow 3P} = \omega_{3D \rightarrow 3S} - \omega_{3P \rightarrow 3S}$ and $\omega_{840} = \omega_{3D \rightarrow 3S} - \omega_L$), it can be seen that an axially phase-matched six-wave mixing photon should be emitted with its wavelength almost midway between those of the 840 and 819 nm emissions.

Use of (5) and (7) including all six photons and resonance terms through the $3S \rightarrow 5P$ doublet allows accurate predictions of the axial six-wave mixing photon wavelengths for a given laser wavelength. Wavelengths calculated in this manner are compared to observed wavelengths in Table 1 for the case of pure sodium vapor and for several laser frequencies. For these calculations, energies and oscillator strengths were taken from [18]. Note that while ω_1 and ω_2 shift with the pump laser wavelength (for a shift $\Delta\omega_L$ of the

pump frequency, we expect $\Delta\omega_1 \equiv \Delta\omega_{584} \approx \Delta\omega_L/2$ and $\Delta\omega_2 \equiv \Delta\omega_{830} \approx -\Delta\omega_L/2$), it is a different dependence than that predicted for the angle phase-matched 840 nm emission ($\Delta\omega_{840} \approx -\Delta\omega_L$) which has recently been demonstrated experimentally by Wang et al. [6] and Yih et al. [20]. Note also that the axially phase-matched emission frequencies ω_1 and ω_2 are independent of the sodium atom density which cancels out of each term in (5).

In addition, it is clear from Fig. 2 that a similar process should occur under the same conditions for the cascade sequence passing through the $4S$ (rather than the $3D$) state. This latter process is responsible for the 1.16 μm emission. Predicted and observed wavelengths for this process are also presented in Table 1.

Finally, we present what is perhaps the most convincing argument in favor of the axially phase-matched six-wave mixing explanation for the 830 nm emission. According to theory, we expect to observe predictable shifts in wavelength of the various emission peaks as we change the refractive index of the vapor. In particular, when we consider the case of these processes occurring in mixed sodium-potassium vapor, we must include the effects of the potassium on the index of refraction. In this case, and again assuming that only the atomic ground states are significantly populated, (7) becomes:

$$n-1 \approx 2\pi \frac{e^2}{m} \left[N_{\text{Na}} \sum_k \frac{f_{ik}}{\omega_{ik}^2 - \omega^2} + N_{\text{K}} \sum_m \frac{f_{jm}}{\omega_{jm}^2 - \omega^2} \right]. \quad (10)$$

Here, states i and j represent the sodium and potassium ground states, respectively. Since the potassium resonance lines lie at 765 and 770 nm, the second term on the right-hand side of (10) contributes significantly to the dispersion in the vicinity of 830 nm. This pushes the 830 nm emission to shorter wavelengths, with the actual value being determined by the relative sodium to potassium density ratio. Qualitatively, this is what we observe in Fig. 10. Note that the analogous emission near 1.16 μm (involving the $4S$ state cascade channel) is not shifted as much in frequency, since the potassium contributes less to the dispersion of either ω_1 or ω_2 in this case.

It is difficult to determine the sodium-potassium density ratio in the heat-pipe oven, because the two species tend to separate [21]. However, we know that an upper limit to $N_{\text{K}}/N_{\text{Na}}$ is ~ 10 which is obtained from vapor pressure curves [22], and a lower limit is clearly zero for complete separation. In Table 2 we present values of the observed positions of the 830 nm and 1.16 μm peaks for two pump wavelengths. These can be compared to tabulated values of the peak positions calculated from (5) and (10) using various values of the ratio $N_{\text{K}}/N_{\text{Na}}$. It can be seen that the shifts agree fairly well with those predicted for $N_{\text{K}}/N_{\text{Na}} \sim 3$.

Table 2. Measured and calculated positions of axially phase-matched six-wave mixing signals in mixed sodium-potassium vapors for two pump laser wavelengths. The calculated values are obtained from (5) and (10) using several values for the ratio N_K/N_{Na} . These ratios are given in the last column. Wavelengths are in air, and are given in nm. The experimental conditions were as in Fig. 10, and the experimental uncertainties are given in parentheses

λ_{pump}	3D channel		4S channel		N_K/N_{Na}
	$\lambda(\omega_1)$	$\lambda(\omega_2)$	$\lambda(\omega_1)$	$\lambda(\omega_2)$	
Experimental					
578.66 (± 0.05)	–	825.26 (± 0.3)	–	1156.75 (± 0.5)	
578.86 (± 0.05)	–	824.84 (± 0.3)	–	1156.31 (± 0.5)	
Theoretical					
578.66	584.05	829.24	584.00	1159.69	0
	584.53	828.28	584.22	1158.84	0.5
	584.93	827.48	584.42	1158.06	1.0
	585.56	826.21	584.76	1156.69	2.0
	586.04	825.27	585.07	1155.52	3.0
	586.41	824.54	585.33	1154.50	4.0
	586.70	823.96	585.56	1153.61	5.0
	586.93	823.50	585.76	1152.81	6.0
	587.30	822.79	586.10	1151.49	8.0
	587.55	822.28	586.39	1150.40	10.0
	578.86	584.15	829.05	584.10	1159.30
584.61		828.12	584.31	1158.49	0.5
584.99		827.35	584.50	1157.74	1.0
585.61		826.12	584.84	1156.43	2.0
586.08		825.19	585.13	1155.28	3.0
586.44		824.48	585.38	1154.29	4.0
586.72		823.92	585.60	1153.42	5.0
586.96		823.46	585.80	1152.65	6.0
587.31		822.77	586.14	1151.34	8.0
587.56		822.27	586.42	1150.28	10.0

This value appears reasonable for the heat-pipe oven. We have also found that variation of the oven temperature and buffer gas pressure can cause the 830 nm peak to move in Na–K mixtures but not in pure sodium. This is because the variation of the mixed-vapor oven operating conditions causes variation in N_K/N_{Na} in the central part of the oven. Clearly, this cannot occur in the pure vapor.

Because of its simple dependence on N_K/N_{Na} , it is possible that the shift of the 830 nm emission can be used as a convenient measure of this ratio in the central region of sodium-potassium heat-pipe ovens. This, and analogous processes in other alkali vapors, might prove useful in determining atom density ratios in various experiments involving spectroscopy of heteronuclear molecules, or the study of collisions between dissimilar atoms.

4. Conclusions and Summary

In the preceding sections, we have presented experimental and theoretical evidence which unambiguously identifies the 830 nm emission, observed under two-

photon pumping of the Na $3S \rightarrow 4D$ transition, as an axially phase-matched six-wave mixing process. This evidence includes the observation of coherent emission at 584 nm, which is coupled to the 830 nm emission in the wave-mixing process, and a related emission peak at 1.16 μm , which is due to an analogous six-wave mixing process involving the 4S intermediate state. The common nature of these three emissions is documented by the similarity of their excitation spectra and their dependences on laser power. The axial nature of this six-wave mixing process has been demonstrated by angle dependent studies carried out with an aperture. In addition, we have observed dramatic shifts in the wavelengths of these axially phase-matched emissions when we changed the refractive index of the vapor by mixing potassium with the sodium.

These observations can be easily explained by a simple model of axially phase-matched six-wave mixing similar to that presented recently by Moore et al. [8,9]. We have used this model to predict the wavelengths of the various emissions in pure sodium vapor, and have obtained values which agree with observations to within experimental uncertainties. This

model also qualitatively explains the wavelength shifts observed in sodium-potassium mixtures. The only parameter needed to make these last calculations quantitative is the ratio of the potassium to sodium number densities. In fact, observations of this type may be useful for obtaining atom density ratios in other experiments on mixed alkalis.

Using this simple model, we can also speculate about the origin of the dip in the axially phase-matched six-wave excitation spectra for resonant pumping. When the pumping is well off resonance, the excited state populations remain small, and the indices of refraction are given by (7) with N_i replaced by N and the sum extending over the $3S \rightarrow nP$ resonance series. However, if the laser is tuned onto resonance, this approximation breaks down, and the conditions for axial phase matching are altered considerably. The indices of refraction will change, due to the increase in the number of excited atoms, and to an increase in ionization, and this could disrupt the axial phase-matching process. An alternate explanation of this dip is competition between the 820, 830, and 840 nm emission processes, with the 820 nm processes dominating the resonant excitation case. We believe that another possible explanation, based on a simple depletion of available sodium atoms by two-photon resonant, three-photon ionization, is incorrect, because this would cause a similar dip in the 820 and 840 nm signals which is not observed. We tried to experimentally distinguish between some of these possibilities by studying the pump laser intensity dependence of the 830 nm excitation spectra which is shown in Fig. 8. We thought the resonance dip might be reduced for lower pump power where the excited atom densities are smaller. In fact, the dip does appear to narrow, and the width of the excitation spectrum is reduced as we decrease the laser power. However, we do not believe that any definite conclusions can be reached concerning the resonance dip at this time.

The simple theory presented here only predicts emission wavelengths for a given pump wavelength, and says nothing about intensities. We have not explained the great breadth of the emission spectrum which can occur under certain circumstances (see [Ref. 16, Fig. 4] in particular). We have also not explained the shape and breadth of the excitation spectra other than to mention some possible explanations for the resonance dip. We hope that the present experimental study will stimulate further theoretical work on these processes which might address the questions of excitation lineshapes, and competition between the processes of ASE, axial phase-matched wave-mixing, and angle phase-matched wave-mixing which can occur simultaneously in this system.

Finally, we believe that the evidence presented above makes it impossible to give further support to

explanations of the 830 nm emission as Na_2 bound-free $1^3\Sigma_g^+ \rightarrow 1^3\Sigma_u^+$ excimer emission, that have appeared recently in the literature [13, 16]. Such explanations cannot explain the presence of a correlated photon at 584 nm, or the analogous emission at $1.16 \mu\text{m}$. In addition, excimer explanations cannot account for the observed shift of the 830 nm emission in Na-K mixtures, both because the shift can be made continuous with variation of the sodium/potassium ratio, and because the analogous excimer bands of the NaK and K_2 molecules occur at wavelengths beyond $1 \mu\text{m}$.

Acknowledgements. We are grateful to M. A. Moore, W. R. Garrett, R. N. Compton, and S. J. Bajic for many helpful discussions and for providing us with their results prior to publication. This work was supported by the Army Research Office under grant DAALO3-86-K-0161 and the National Science Foundation under grant PHY-8451279.

References

1. D. Cotter, D.C. Hanna, W.H.W. Tuttlebee, M.A. Yuratich: *Opt. Commun.* **22**, 190 (1977)
2. W. Hartig: *Appl. Phys.* **15**, 427 (1978)
3. P.-L. Zhang, Y.-C. Wang, A.L. Schawlow: *J. Opt. Soc. Am. B* **1**, 9 (1984)
4. J. Krasinski, D.J. Gauthier, M.S. Malcuit, R.W. Boyd: *Opt. Commun.* **54**, 241 (1985)
5. S.M. Hamadani, J.A.D. Stockdale, R.N. Compton, M.S. Pindzola: *Phys. Rev. A* **34**, 1938 (1986)
6. Z.G. Wang, H. Schmidt, B. Welleghausen: *Appl. Phys. B* **44**, 41 (1987)
7. M.A. Moore, W.R. Garrett, M.G. Payne: *Opt. Commun.* **68**, 310 (1988)
8. M.A. Moore, W.R. Garrett, M.G. Payne: *Phys. Rev. A* **39**, 3692 (1989)
9. M.A. Moore: Ph.D. dissertation, University of Tennessee (unpublished)
10. B. Welleghausen: *IEEE J. QE-15*, 1108 (1979)
11. K.K. Verma, J.T. Bahns, A.R. Rajaei-Rizi, W.C. Stwalley: *J. Chem. Phys.* **78**, 3599 (1983)
12. J.T. Bahns, K.K. Verma, A.R. Rajaei-Rizi, W.C. Stwalley: *Appl. Phys. Lett.* **42**, 336 (1983)
13. S.G. Dinev, I.G. Koprnikov, I.L. Stefanov: *Opt. Commun.* **52**, 199 (1984)
14. D.D. Konowalow, P.S. Julienne: *J. Chem. Phys.* **72**, 5815 (1980)
15. J. Huennekens, S. Schaefer, M. Ligare, W. Happer: *J. Chem. Phys.* **80**, 4794 (1984)
16. S.J. Bajic, R.N. Compton, J.A.D. Stockdale, D.D. Konowalow: *J. Chem. Phys.* **89**, 7056 (1988)
17. D. Veza, J. Rukavina, M. Movre, V. Vujnovic, G. Pichler: *Opt. Commun.* **34**, 77 (1980)
18. W.L. Wiese, M.W. Smith, B.M. Miles: *Atomic Transition Probabilities*, Vol. II, NSRDS-NBS 22 (1969)
19. M. Born, E. Wolf: *Principles of Optics* (Pergamon, Oxford 1980) pp. 87-94
20. T.S. Yih, H.H. Wu, Y.C. Hsu, K.C. Lin: In *Advances in Laser Science III*, ed. by A.C. Tam, J.L. Gole, and W.C. Stwalley (American Institute of Physics, New York 1988) pp. 161-163
21. M.M. Hessel, P. Jankowski: *J. Appl. Phys.* **43**, 209 (1972)
22. A.N. Nesmeyanov: *Vapor Pressure of the Elements* (Academic, New York 1963)